Advanced Composite Materials
Publication details, including instructions for authors and subscription information:
http://www.tandfonline.com/loi/tacm20

Strength Prediction Method for Unidirectional GFRP after Hydrothermal Aging

Masahiro Kotani [a], Yohei Yamamoto [b], Youhei Shibata [c] & Hiroyuki Kawada [d]

[a] Department of Mechanical Engineering, Waseda University, 3-4-1 Okubo, Shinjuku-ku, Tokyo 169-8555, Japan, Graduate School of Waseda University, 3-4-1 Okubo, Shinjuku-ku, Tokyo 169-8555, Japan;, Email: robot_5ta2@toki.waseda.jp

[b] Graduate School of Waseda University, 3-4-1 Okubo, Shinjuku-ku, Tokyo 169-8555, Japan

[c] Graduate School of Waseda University, 3-4-1 Okubo, Shinjuku-ku, Tokyo 169-8555, Japan

[d] Department of Mechanical Engineering, Waseda University, 3-4-1 Okubo, Shinjuku-ku, Tokyo 169-8555, Japan

Version of record first published: 02 Apr 2012.

To cite this article: Masahiro Kotani , Yohei Yamamoto , Youhei Shibata & Hiroyuki Kawada (2011): Strength Prediction Method for Unidirectional GFRP after Hydrothermal Aging, Advanced Composite Materials, 20:6, 519-535

To link to this article: http://dx.doi.org/10.1163/156855111X595855

VSP

Advanced Composite Materials 20 (2011) 519–535

ADVANCED COMPOSITE MATERIALS
brill.nl/acm

Strength Prediction Method for Unidirectional GFRP after Hydrothermal Aging

Masahiro Kotani [a,b,*], **Yohei Yamamoto** [b], **Youhei Shibata** [b] **and Hiroyuki Kawada** [a]

[a] Department of Mechanical Engineering, Waseda University, 3-4-1 Okubo, Shinjuku-ku, Tokyo 169-8555, Japan

[b] Graduate School of Waseda University, 3-4-1 Okubo, Shinjuku-ku, Tokyo 169-8555, Japan

Received 7 October 2010; accepted 27 July 2011

Abstract

This paper proposes a strength prediction method for unidirectional glass fiber reinforced plastics (GFRPs) after hydrothermal aging: immersion in deionized water at 80°C. First, the strength degradation of the constituents (i.e., the glass fiber and the fiber/matrix interface) of unidirectional GFRP after hydrothermal aging was evaluated from the fiber strength and the interfacial shear stress by using a single-fiber composite (SFC). Both the fiber strength and the interfacial shear stress had a tendency to decrease in the early stage of hydrothermal aging and to saturate toward certain values with long-term aging. In addition, the tensile strength of the unidirectional GFRP was measured after hydrothermal aging. The residual strength of the unidirectional GFRP also had a tendency to decrease sharply in the early stage of hydrothermal aging and to saturate toward a certain strength with long-term aging. Finally, the residual strength of the unidirectional GFRP after hydrothermal aging was predicted using the global loading sharing (GLS) model, by considering the degradation of both the glass fiber and the fiber/matrix interface. The predicted results indicated good agreement with the experimental data while considering not only the degradation of the fiber reinforcement but also the fiber/matrix interface adhesion. It was concluded that the GLS model applied considering the degradation of the GFRP constituents would be a suitable and a simple model to predict the residual strength of the unidirectional GFRP after hydrothermal aging.

Keywords

GFRP, hydrothermal aging, strength prediction, interfacial degradation, global load sharing

1. Introduction

Glass fiber reinforced plastics (GFRPs) have superior corrosive resistance compared to metal materials and have various applications, such as material for con-

* To whom correspondence should be addressed. E-mail: robot_5ta2@toki.waseda.jp
Edited by the JSCM

DOI:10.1163/156855111X595855

structing wind turbine blades, industrial facilities, and marine structures. In fact, GFRPs operating in a corrosive environment are designed with excessive safety factors due to the lack of long-term reliability data. Unfortunately, some accidents involving GFRPs operating in corrosive environments have been reported. Such accidents occur due to the strength degradation of GFRP, for example, stress corrosion cracking (SCC) that is generated by the interaction between mechanical factors and environmental agents. Therefore, it is an urgent task to clarify the failure mechanism of GFRP in a corrosive environment in order to assure its long-term reliability and to guarantee its widely spreading application fields.

The majority of the previous studies on GFRP operating in corrosive environments have focused on the macroscopic degradation, such as crack propagation and reduction in the mechanical properties after exposure to a corrosive environment and were conducted using GFRP laminates [1, 2]. Kawada and Kobiki investigated the crack propagation in GFRP laminates in deionized water and a vitriolic environment and concluded that the influence of the solution against crack propagation strongly depends on the diffusion of water molecules: they suggested the existence of a threshold stress intensity factor K_{ISCC} similar to that in the case of metal materials [3]. On the other hand, the strength degradation of GFRP in corrosive environments has been investigated by various researchers [4–6]. Liao *et al.* conducted tensile tests and flexural tests using pultruded GFRP after environmental aging in various solutions and examined the aging effect on the failure mechanism [4]. The transition in the fracture surface due to the degradation of the constituents was ascertained; however, the relationship between the degradation of GFRP and its constituents remains uncertain. It is therefore required to propose a numerical method that can be used to calculate the variation in the residual strength of GFRP from the strength of the constituents after environmental aging.

In this study, the residual strength of unidirectional GFRP after hydrothermal aging was investigated, and a strength prediction method considering the degradations of its constituents was proposed. The hydrothermal aging in the present paper was carried out in deionized water at 80°C so as to accelerate the degradation. First, fiber fragmentation tests were conducted on a single-fiber composite (SFC) specimen after hydrothermal aging in order to evaluate the strength degradation of the glass fiber and fiber/matrix interface. Subsequently, tensile tests were conducted on the unidirectional GFRP in order to measure its residual strength after hydrothermal aging. Finally, the residual strength of the unidirectional GFRP after hydrothermal aging was calculated based on the assumption of the global load sharing (GLS) considering the strength degradation of the glass fiber and the adhesion of the fiber/matrix interface. The swelling stresses of the resin matrix due to the water absorption in the fiber radius direction were installed into the stress analysis of the existing model. On the basis of the obtained results, the influence of the fiber/matrix interface on the residual strength of the unidirectional GFRP will be discussed in this paper.

2. Experimental

2.1. Specimens

The specimens were a dumbbell-shaped single fiber composite (SFC) specimen and a bar-shaped unidirectional GFRP specimen. For convenience of identification, hereafter in this paper, the dumbbell-shaped SFC is referred to as the 'SFC specimen' and the unidirectional GFRP is referred to as the 'UD specimen'. A single filament of NCR-glass was embedded in the SFC, and NCR-glass tows were embedded in the UD specimen. For the SFC specimen, the single filament was separated from a tow of fibers and was placed into a dumbbell-shaped mold. Pre-tension was applied to the embedded glass fiber in order to compensate for the curing shrinkage of the resin matrix. Each specimen was fabricated by casting using a specimen-shaped mold. The constituents and the geometries of both specimens are listed in Table 1 and shown in Fig. 1. The curing condition of the vinylester resin was carried out for 3 h at 25°C, and post-curing was conducted for 2 h at 120°C. These curing conditions were determined from the differential scanning calorimetry (DSC) test of neat vinylester resin. Furthermore, a waterproof sheathing was applied on both

Table 1.
Mechanical properties of GFRP constituents

	NCR-Glass	Vinylester
Young's modulus E (GPa)	72.5	3.00
Diameter d (μm)	23.5	—
Poisson's ratio ν	0.14	0.32

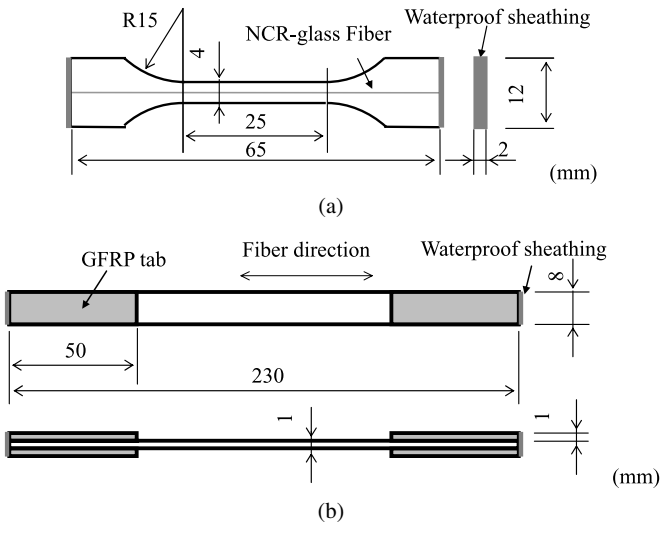

Figure 1. Geometry of GFRP specimens. (a) Single fiber composite. (b) Unidirectional GFRP.

specimens to prevent the direct water penetration from the exposed fiber/matrix interface at each specimen edge.

The present study assumes that the Young's modulus of the NCR-glass E^{f} does not change after hydrothermal aging [7]. The average fiber-volume fraction V_{f} of the unidirectional GFRP was approximately 30%. In this presentation, the superscript 'f' stands for the fiber reinforcement; 'm' for the resin matrix; 'i' for the fiber/matrix interface; 'SFC' for the SFC specimen; and 'UD' for unidirectional GFRP.

2.2. Water Absorption Test

The degradations of the fiber reinforcement and fiber/matrix interface begin at the moment the water diffusion reaches the fiber surface through the surrounding matrix. In addition, the resin matrix swells with water absorption. Water absorption tests were conducted in order to evaluate these water uptake properties for each specimen. The bar-shaped specimen (140 mm × 20 mm × t2 mm) made of neat vinylester resin and the unidirectional GFRP were immersed in deionized water at 80°C, and their weight $M(t)$ and the elongation in the longitudinal direction $L(t)$ were measured. The weight gain ΔM and the swelling strain $\varepsilon_{\mathrm{swell}}$ were evaluated using following equations:

$$\Delta M = \frac{M(t) - M(0)}{M(0)}, \tag{1}$$

$$\varepsilon_{\mathrm{swell}} = \frac{L(t) - L(0)}{L(0)}. \tag{2}$$

2.3. Fiber Fragmentation Test on SFC

On the SFC specimen, fiber fragmentation tests were conducted in air at room temperature after hydrothermal aging so as to evaluate the degradation of the GFRP constituents. The number of fiber break points n, applied strain ε^{f}, and interfacial debonding length L_{d} were measured during the fiber fragmentation test. Tensile loading was introduced by means of a compact testing machine with a 2 kN capacity, and the test speed was 0.1 mm/min. A strain gage was bonded to the gage section in order to measure the axial strain during the test. The fiber break point was enhanced using the polarizing effect, and the point with the maximum brightness was determined as the interfacial debonding tip by using image processing. Therefore, it was possible to evaluate the interfacial debonding length L_{d} quantitatively. The equipment used in the fiber fragmentation test is shown in Fig. 2 and the photograph of interfacial debonding in the vicinity of fiber break point is shown in Fig. 3.

2.4. Tensile Test of Unidirectional GFRP

On the UD specimen, tensile tests were conducted in air at room temperature after hydrothermal aging, to evaluate the degradation of mechanical properties. Loading was introduced by means of a 10 kN capacity testing machine and the constant

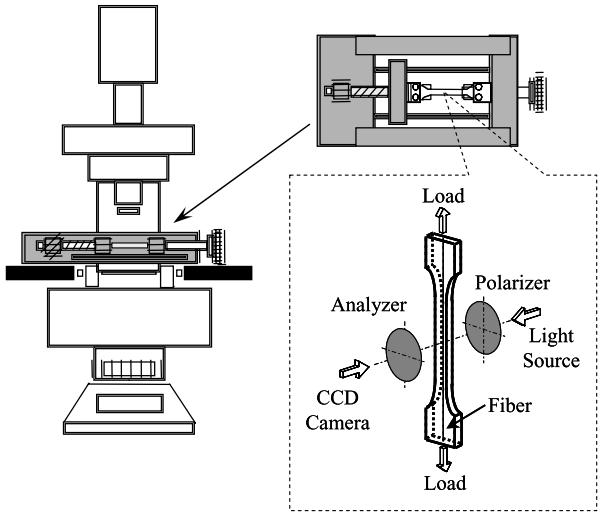

Figure 2. Illustration of equipment used for the fiber fragmentation test.

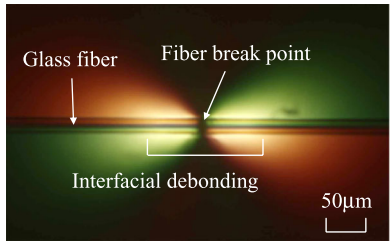

Figure 3. Photograph of interfacial debonding in the vicinity of fiber break point through polarizing plate. This figure is published in color in the online version.

cross-head rate was 0.1 mm/min. A strain gage was bonded on the gage section so as to measure the axial strain during the tensile test.

3. Results and Discussion

3.1. Water Absorption Behavior

The water absorption behavior of neat vinylester resin (ε^{m}_{swell} and ΔM) was studied from the results of the water absorption test and is shown in Fig. 4. The water uptake of neat vinylester resin results exhibits the Fickian behavior in which the water uptake increases in the early stage of water immersion and to saturate toward a certain value. The immersion time required to attain the saturation was about 20 h and the swelling strain was determined to be $\varepsilon^{m}_{swell} = 0.20\%$ after saturation. In addition, the swelling strain in the UD specimen ε^{UD}_{swell} was negligible after water immersion. This is due to the restraint of the glass fiber against the swelling of the resin matrix that is aligned in the longitudinal direction [8]. These results would

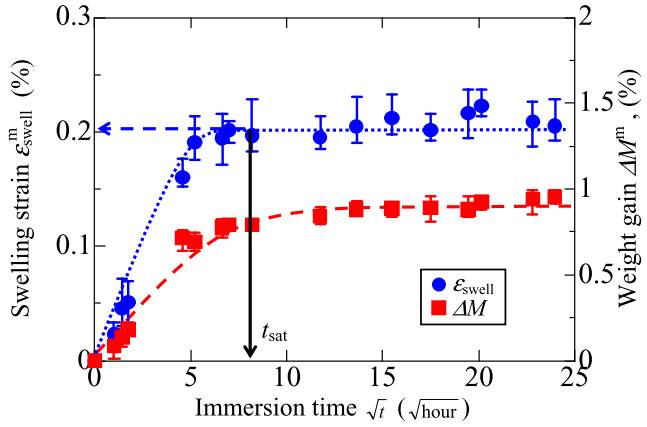

Figure 4. Water uptake of vinylester resin matrix. This figure is published in color in the online version.

be substituted into the stress analysis to calculate the strength of the UD specimen which will be presented later.

3.2. Fiber Strength Degradation

The fiber-volume fraction for the SFC specimen is minute ($V_f \approx 0.01\%$) so that the embedded glass fiber expands together with its surrounding resin matrix [7]. Therefore, the strain applied to the embedded fiber ε^f is expressed as follows:

$$\varepsilon^f = \varepsilon^{SFC}_{app} + \varepsilon^m_{swell}, \tag{3}$$

where ε^{SFC}_{app} denotes the strain applied to the SFC specimen by the testing machine. The residual strength distribution of the embedded glass fiber was measured by the fiber fragmentation test and is shown in Fig. 5. The fiber strength distribution would be evaluated by means of a two-parameter Weibull distribution by using the following equation [8]:

$$\ln n = \frac{L}{L_0}\left(\frac{E^f \varepsilon^f}{\sigma_0}\right)^m, \tag{4}$$

where n signifies the number of fiber break points, L is the gage length (= 25 mm), L_0 is the reference length (= 25 mm), σ_0 is the scale parameter, and m is the shape parameter. The interfacial debonding occurs in the vicinity of fiber break point and the influence of the interfacial debonding length on the reference length has to be considered. Thus, the effective length L' which considers the effect of the interfacial debonding length was adopted. The correlated effective length L' at strain ε is calculated from the following equation [9]:

$$L' = L_0 \times \left(1 - \frac{4}{3}\frac{1}{n_c + 1}\frac{\varepsilon}{\varepsilon_c}\right), \tag{5}$$

where n_c and ε_c are the number of fiber break points and applied strain required to obtain the critical fragment state, which are obtained from the fiber fragmentation

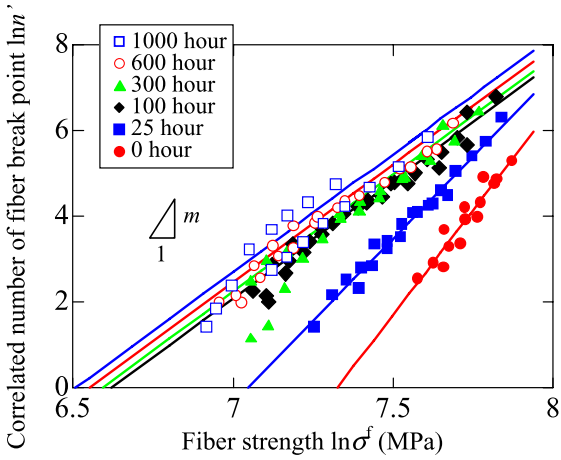

Figure 5. Strength distribution of embedded NCR-glass fiber after hydrothermal aging obtained from fiber fragmentation test. This figure is published in color in the online version.

Table 2.
Weibull parameters obtained from fiber fragmentation test

Aging time t (h)	0	25	100	300	600	1000
m	9.8	7.8	5.4	5.4	5.3	5.3
σ_0 (MPa)	1500	1200	740	730	700	660

test. The second term in the right side expresses the interfacial debonding length in the reference length. By considering the effect of the interfacial debonding length on the gage length L, the correlated number of fiber break points n' and the corrected effective length L' would be expressed as follows [9]:

$$\frac{L_0}{n'+1} = \frac{L'}{n+1}. \tag{6}$$

Thus, we obtain the relationship between the correlated number of fiber break points n' and the Weibull distribution as the following equation:

$$\ln n' = \frac{L'}{L_0}\left(\frac{\sigma^{\mathrm{f}}}{\sigma_0}\right)^m. \tag{7}$$

The Weibull parameters σ_0 and m used in the fiber strength distribution are listed in Table 2, and the fitted lines are shown in Fig. 5.

It is obvious from the scale parameter σ_0 that the residual strength of the embedded glass fiber decreases drastically in the early stage of hydrothermal aging (until 100 h), and that it saturates toward a certain strength with long-term aging (namely 45% of the initial strength). It is also obvious that the dispersion of strength distribution, which is represented by in the scale parameter m, seems to increase with the aging time. The glass fiber strength depends on the pre-existing surface flaws,

which originate with various sizes during the manufacturing process. The combined effect of the applied stress and the aging on the embedded fiber leads to the growth of the surface flaws. The growth rate of a surface flaw increases with its size; therefore, the range of the flaw size distribution enlarges, resulting in a decrease in the shape parameter m.

3.3. Interfacial Strength Degradation

In this paper, the fiber/matrix interfacial strength is discussed in terms of the interfacial shear stress τ^{i}, which is calculated employing elastic analysis. Figure 6 shows the elastic analysis model applied in the vicinity of the fiber break point considering the swelling stresses of the resin matrix due to water absorption (axial stress $\sigma^{\mathrm{m}}_{z,\mathrm{swell}}(t)$ and radial stress $\sigma^{\mathrm{m}}_{r,\mathrm{swell}}(t)$). The interfacial shear stress τ^{i} and the axial fiber stress σ^{f} are expressed by the following equations [10, 11]:

(i) $0 \leqslant z \leqslant L_d$

$$\tau^{\mathrm{i}}(z) = \left(H_1 - \mu\sigma^{\mathrm{m}}_{r,\mathrm{swell}}(t)\right)\exp(-\alpha z), \tag{8}$$

$$\sigma^{\mathrm{f}}(z) = \frac{H_1}{H_2}(1 - \exp(-\alpha z)). \tag{9}$$

(ii) $L_d < z$

$$\tau^{\mathrm{i}}(z) = \tau^{\mathrm{i}}_{\max}\exp\beta(L_{\mathrm{d}} - z), \tag{10}$$

$$\sigma^{\mathrm{f}}(z) = \sigma^{\mathrm{f}}_0 + \sigma^{\mathrm{m}}_{z,\mathrm{swell}}(t) - \frac{4\tau^{\mathrm{i}}_{\max}}{\beta d^{\mathrm{f}}}\exp\beta(L_{\mathrm{d}} - z), \tag{11}$$

where $\mu(= 0.7$ [13]) denotes the coefficient of friction, σ^{f}_0 represents the axial stress

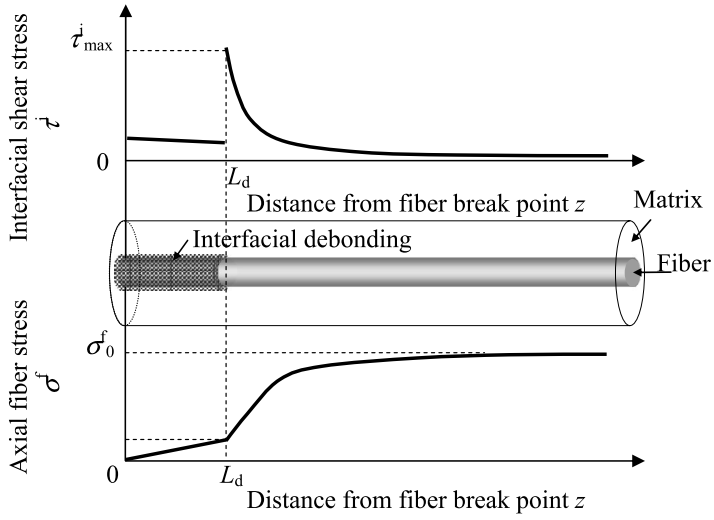

Figure 6. Elastic analysis model and stress distribution considering interfacial debonding.

Table 3.
Swelling stresses after hydrothermal aging [12]

Aging time t (h)	Swelling strain $\varepsilon_{\text{swell}}$ (MPa)	Swelling stress (MPa)	
		$\sigma^{\text{m}}_{r,\text{swell}}$	$\sigma^{\text{m}}_{z,\text{swell}}$
0	0	—	—
20∼	0.20	−1.65	−12.2

in a remote unbroken fiber, H_1 is a function of σ^{f}_0, H_2, α and β are constants. $\sigma^{\text{m}}_{r,\text{swell}}$ and $\sigma^{\text{m}}_{z,\text{swell}}$ signify the swelling stresses induced by the swelling resin matrix after hydrothermal aging and is described in Table 3 [12]. The constants H_1, H_2, α and β are given by the following equations:

$$H_1 = \frac{\mu \nu^{\text{m}} E^{\text{m}} (\sigma^{\text{f}}_0 + \sigma^{\text{m}}_{z,\text{swell}}(t))}{(1-\nu^{\text{f}})E^{\text{m}} + (1+\nu^{\text{m}})E^{\text{f}}}, \tag{12}$$

$$H_2 = \frac{\mu \nu^{\text{f}} E^{\text{m}} E^{\text{f}}}{(1-\nu^{\text{f}})E^{\text{m}} + (1+\nu^{\text{m}})E^{\text{f}}}, \tag{13}$$

$$\alpha = \frac{4H_2}{d^{\text{f}}}, \tag{14}$$

$$\beta = \sqrt{\frac{4G^{\text{m}}}{d^{\text{f}} t^{\text{m}} E^{\text{f}}}}, \tag{15}$$

where ν^{f} and ν^{m} indicate the Poisson's ratio of the glass fiber and the vinylester resin, respectively, d^{f} denotes the fiber diameter, G^{m} represents the shear modulus of the vinylester resin, and t^{m} specifies the distance between the adjacent fibers. t^{m} is calculated from the fiber-volume fraction V_{f}, as expressed in the following equation:

$$t^{\text{m}} = d^{\text{f}} \left(\sqrt{\frac{\pi\sqrt{3}}{6V_{\text{f}}} - 1} \right). \tag{16}$$

The interfacial shear stress which assumes the maximum value at the interfacial debonding tip $\tau^{\text{i}}_{\max}$, is determined by the following equation:

$$\tau^{\text{i}}_{\max} = \frac{\beta d^{\text{f}}}{4} \left[\sigma^{\text{f}}_0 + \sigma^{\text{m}}_{z,\text{swell}} - \frac{H_1}{H_2}(1 - \exp(-\alpha L_{\text{d}})) \right], \tag{17}$$

where the parameters, σ^{f}_0 and L_{d}, were obtained from the fiber fragmentation test. The aging time variation in the maximum shear stress $\tau^{\text{i}}_{\max}$ is shown in Fig. 7. The figure depicts that the interfacial strength (maximum shear stress) decreases in the early stage of hydrothermal aging and seems to saturate toward a certain strength with long-term aging — reduction to 60% of its initial strength. Possible

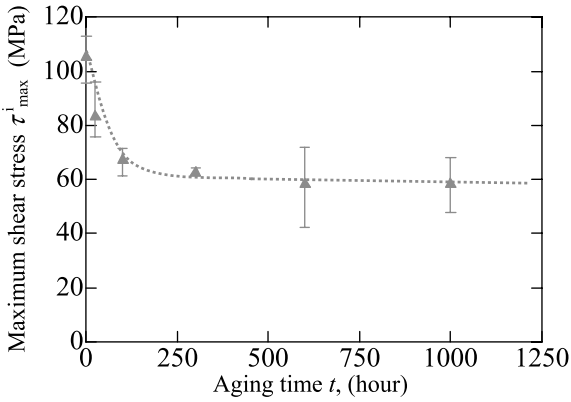

Figure 7. Maximum interfacial shear strength after hydrothermal aging obtained from fiber fragmentation test.

Table 4.
Material properties of unidirectional GFRP after hydrothermal aging

Aging time t (h)	Residual strength σ_{UTS} (MPa)	Rupture strain ε (%)	Stiffness E (GPa)
0	440	1.79	25
25	350	1.14	27
100	280	1.18	29
300	250	0.88	30
600	250	0.78	31
1000	240	0.82	31

factors responsible for this decreasing trend may be: (i) the equilibrium states in the hydrolysis of the silane-coupling agent, and (ii) the saturation of the swelling strain due to water absorption.

3.4. Residual Strength of Unidirectional GFRP

Tensile tests were conducted on the unidirectional GFRP in order to determine its residual strength after hydrothermal aging, and the results are described in Table 4. The stress–strain curves of the UD specimen at various aging times are shown in Fig. 8, and the relationship between the residual strength and the aging time are highlighted in Fig. 9.

The residual strength and rupture strain of the UD specimen decrease in the early stage of hydrothermal aging and seem to saturate toward certain values with long-term immersion. This is natural because the constituents of the UD specimen had similar strength degradation behavior, which is evaluated in terms of σ_0^{f} and τ_{max}^{i}. In contrast, the stiffness of the UD specimen increased slightly after hydrothermal aging. The stiffness of the UD specimen are determined by the stiffness of

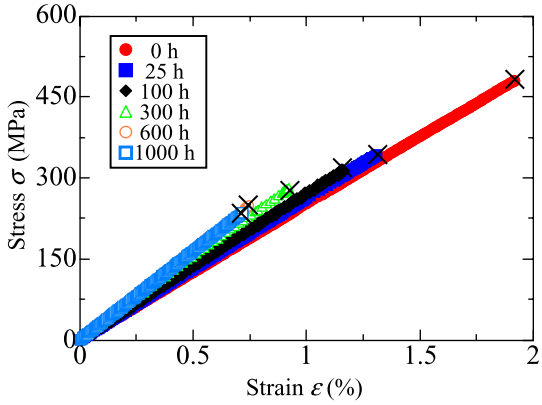

Figure 8. Stress–strain curve of unidirectional GFRP after hydrothermal aging. This figure is published in color in the online version.

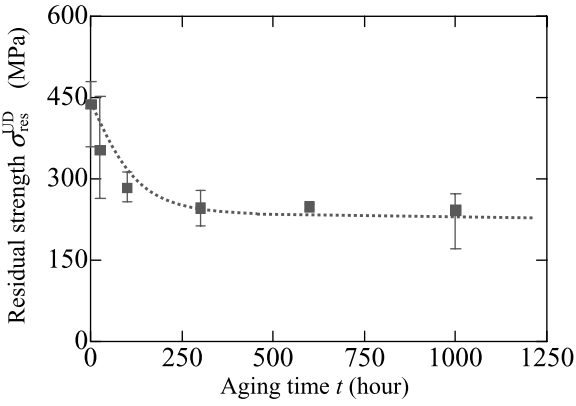

Figure 9. Residual strength of unidirectional GFRP after hydrothermal aging.

the glass fiber and resin matrix, and moreover by the stress transfer between the fiber/matrix interface [14]. The decrease of the stiffness of the glass fiber is thought to be negligible because the hydrothermal aging only occurs on the fiber surface, which will not affect the constituents of the glass fiber as a whole. The degradation of the vinylester resin matrix was negligible in the range of this research [8]. Thus, the increase of the stiffness is concluded to be induced by the degradation of the fiber/matrix interface. In fact, it is reported in previous researches that the strength and the stiffness of the unidirectional composite increases with the decrease in the fiber/matrix interface [14]. This phenomenon can be ascertained in the difference in the decrease of the strength. The glass fiber strength σ_0^f decreased to 43% of its initial strength, the UD specimen retained 60% of its initial strength.

The fracture surface of the UD specimen is shown in Fig. 10. Resin adhesion on the fiber surface and fiber bundle fracture, which is an evidence of strong fiber/matrix interfacial adhesion, can be ascertained from the fracture surface with-

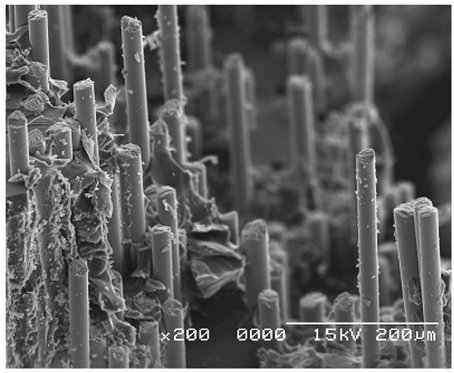

(a)

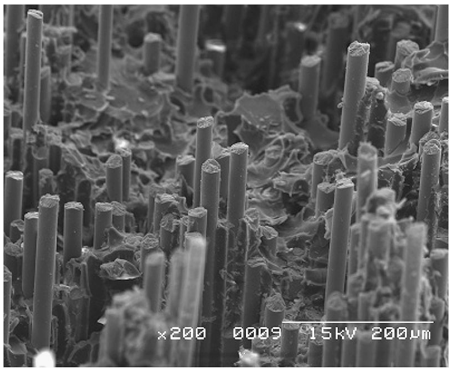

(b)

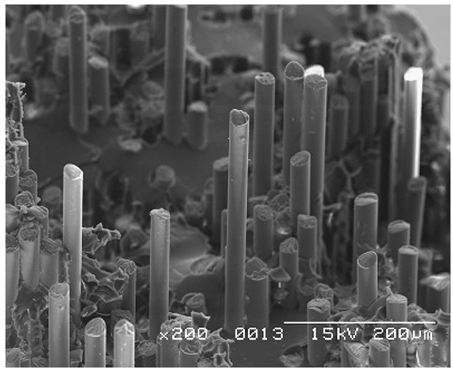

(c)

Figure 10. Fracture surface observation of unidirectional GFRP with various aging time. (a) $t = 0$ (h). (b) $t = 300$ (h). (c) $t = 600$ (h).

out hydrothermal aging (Fig. 10(a)). In contrast, fiber pull-out fracture which is an evidence of poor interfacial adhesion, can be seen on the fracture surface after hydrothermal aging (Fig. 10(b) and (c)). From this transition of the fracture modes, a decrease in the interfacial strength can be verified.

3.5. Strength Prediction of Unidirectional GFRP after Hydrothermal Aging

The residual strength was predicted on the basis of the global load sharing (GLS) model, which is a simplified strength calculation model particularly suitable for unidirectional FRPs with weak interfacial adhesion [13]. In this paper, the interfacial strength decreases with hydrothermal aging, resulting in the relaxation of the strength concentration in the intact unbroken fiber around the broken one. This phenomenon agrees with the assumption of the GLS model; it is therefore suggested that the GLS model would be valid for strength prediction of unidirectional GFRP, particularly after long-term hydrothermal aging. In fact, the strengths of the NCR-glass fiber and fiber/matrix interface degrade with hydrothermal aging; hence these

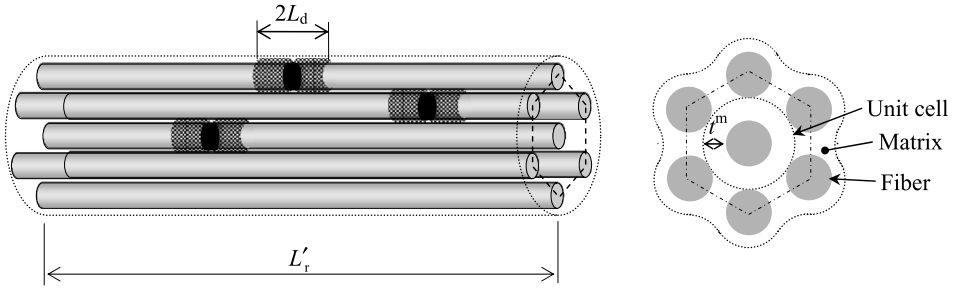

Figure 11. Representative volume element (RVE) of unidirectional GFRP.

strengths which were obtained by conducting the fiber fragmentation tests on the SFC specimen, were integrated into the GLS model.

The residual strength of the UD specimen was predicted as follows. The representative volume element (RVE) for the GLS model is shown in Fig. 11. The stress recovery length L'_r in the vicinity of the fiber break point, considering the interfacial debonding length, is expressed by the following equation:

$$L'_r = L_r + 2L_d, \tag{18}$$

where L_r denotes the stress recovery length, ignoring the interfacial debonding length. At the interfacial debonding tip ($z = L_d$) equations (9) and (11) satisfy the continuity condition, and therefore, the debonding length would be derived as the following equation:

$$L_d = -\frac{1}{\alpha}\ln\left[1 - \frac{H_2}{H_1}\left(\sigma_0^f + \sigma_{z,\text{swell}}^m - \frac{4\tau_{\max}^i}{\beta d^f}\right)\right]. \tag{19}$$

The swelling stress $\sigma_{z,\text{swell}}^m$ and the maximum interfacial shear stress $\tau_{\max}$ were obtained from the water absorption test and the fiber fragmentation test, which varies with the aging time [12]. The average strength of the glass fiber in unidirectional GFRP, evaluated by the GLS model would be expressed as the following equation:

$$\sigma_{\text{ave}}^f = \sigma^f[1 - P(\sigma^f)] + \sigma_b^f\left(\frac{L'_r}{4}\right)P(\sigma^f), \tag{20}$$

where $\sigma_b^f(\frac{L'_r}{4})$ represents the average stress in the broken fiber and $P(\sigma^f)$ indicates the cumulative probability of fiber failure, as expressed in the following equations, respectively [10]:

$$\sigma_b^f\left(\frac{L'_r}{4}\right) = \frac{H_{1i}}{H_{2i}}\left(1 - \exp\left(-\alpha\frac{L_r + 2L_d}{4}\right)\right), \tag{21}$$

$$P(\sigma^f) = 1 - \exp\left[-\frac{L'_r}{L_0}\left(\frac{\sigma^f}{\sigma_0^f}\right)\right]. \tag{22}$$

Thus, we obtain the average strength of the glass fiber as following equation:

$$\sigma_{\mathrm{ave}}^{\mathrm{f}} = \sigma^{\mathrm{f}} \exp\left(-\frac{L_{\mathrm{r}} + 2L_{\mathrm{d}}}{L_0}\left(\frac{\sigma^{\mathrm{f}}}{\sigma_0^{\mathrm{f}}}\right)^m\right) + \frac{H_{1\mathrm{i}}}{H_{2\mathrm{i}}}\left(1 - \exp\left(-\alpha\frac{L_{\mathrm{r}} + 2L_{\mathrm{d}}}{4}\right)\right) \times \left(1 - \exp\left(-\frac{L_{\mathrm{r}} + 2L_{\mathrm{d}}}{L_0}\left(\frac{\sigma^{\mathrm{f}}}{\sigma_0^{\mathrm{f}}}\right)^m\right)\right). \tag{23}$$

In addition, the residual strength of the unidirectional GFRP $\sigma_{\mathrm{res}}^{\mathrm{UD}}$ is given by the rule of mixture as following equation:

$$\sigma_{\mathrm{res}}^{\mathrm{UD}} = \sigma_{\mathrm{ave}}^{\mathrm{f}}\left[\, V_{\mathrm{f}} + (1 - V_{\mathrm{f}})\frac{E^{\mathrm{m}}}{E^{\mathrm{f}}} \,\right]. \tag{24}$$

The strengths of the constituents (σ_0^{f} and $\tau_{\mathrm{max}}^{\mathrm{i}}$) obtained from the fiber fragmentation test were substituted into equation (19), and the residual strength was calculated.

A comparison of the predicted results and the experimental data for residual strength after hydrothermal aging is presented in Fig. 12. The figure depicts that both the predicted results decrease in the early stage of hydrothermal aging and saturate toward a certain strength. Such decreasing trend is natural because the strength of the constituents, namely, the fiber reinforcement and the fiber/matrix interface, also exhibit similar decreasing trend. The glass fiber strength after long-term hydrothermal aging decreased to 43% of its initial strength, and the predicted strength ignoring and considering the decrease in the interfacial strength decreased to 63 and 47% of its initial value, respectively. It is reported by previous researchers that the

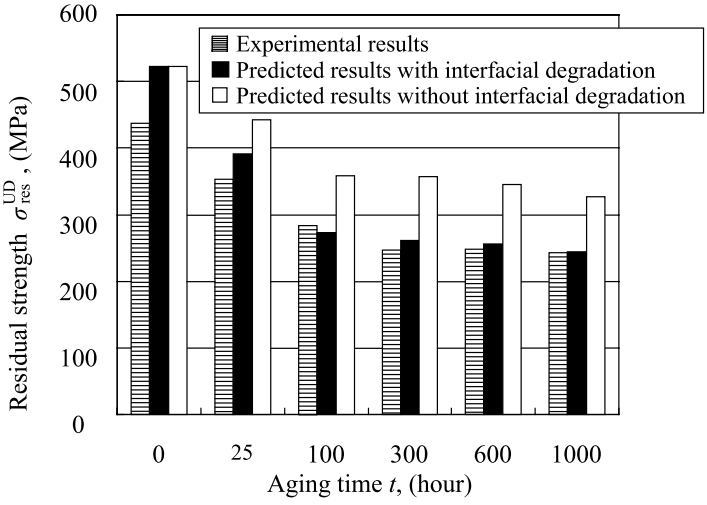

Figure 12. Predicted residual strength of unidirectional GFRP after hydrothermal aging.

strength of unidirectional FRP varies with those of the matrix and the fiber/matrix interface. In particular, for the fiber/matrix interface, the strength of unidirectional FRP first increases with the interfacial strength, attains a maximum, and then decreases [13]. It is suggested that the interfacial strength reported in the present paper was lower than the inflection point, so that the consideration of the decrease in the interfacial strength led to a decrease in the predicted strength.

The assumption of the GLS is widely used in the composites with weak interface such as the C/C composite. This assumption ignores the stress concentration around the broken fiber. If the fiber/matrix interfacial adhesion is weak, the stress concentration releases to the fiber/matrix interface, i.e., propagation of the interfacial debonding. In contrast, in the composite with strong interfacial adhesion, matrix crack and another fiber break at the neighboring fiber occur in the vicinity of the fiber break point and increase the stress concentration around the fiber break point. This causes the composite to fracture within the low strength range. Indeed, both the predicted results within short immersion time $t = 0$ and 25 h are higher than the experimental results. Both the predicted strengths are calculated based on the assumption that the stress concentration releases to the interface and therefore give higher strength. In addition, the predicted results show good agreement with the experimental data particularly after long-term aging by considering the interfacial degradation. It is obvious that the interfacial strength degradation reduces the stress concentration in the vicinity of the broken fiber and leads to a condition that agrees with the assumption of the GLS model. Thus, it is concluded that the strength of the unidirectional GFRP after long-term hydrothermal aging could be predicted by the GLS model by considering the strength degradation of the glass fiber and the fiber/matrix interface.

4. Conclusion

In order to evaluate the strength degradation of an NCR-glass/vinylester composite and its constituents, tensile tests and fiber fragmentation tests were conducted on unidirectional GFRP and SFC specimen, respectively, after hydrothermal aging — hot water immersion at 80°C. Residual strength of the unidirectional GFRP after hydrothermal aging was predicted using the global load sharing model by considering the strength degradation of its constituents. The following conclusions were drawn from the results of this study:

i. Water absorption tests were conducted to evaluate the water uptake of the vinylester resin and the unidirectional GFRP. The weight gain and the swelling strain of vinylester resin followed Fickian behavior: increase in the early stage and saturation after long-term immersion. In contrast, swelling strain of unidirectional GFRP was negligible after water immersion.

ii. Fiber fragmentation tests were conducted on the SFC specimen after hydrothermal aging in order to evaluate the NCR-glass fiber strength and the fiber/matrix

interfacial strength. Both the strengths exhibited similar degradation behavior: extensive decrease in the early stage of hydrothermal aging and saturation toward a certain strength after long-term aging.

iii. Tensile tests were conducted on the unidirectional GFRP after hydrothermal aging so as to evaluate the degradation of its mechanical properties. The residual strength and the rupture strain of the unidirectional GFRP decreased drastically in the early stage of hydrothermal aging and saturated toward certain values after long-term aging.

iv. The residual strength of the unidirectional GFRP was predicted using the global load sharing model by considering the degradation of its constituents: fiber strength and fiber/matrix interfacial strength. By considering the degradation of both of the fiber reinforcement and the fiber/matrix interface, the residual strength of the unidirectional GFRP after hydrothermal aging was predicted in good agreement with the experimental data.

Acknowledgement

This work was supported as a part of Reports of Grants-in-Aid for Scientific Research (C) No. 20560089.

References

1. J. N. Price and D. Hull, Propagation of stress corrosion cracks in aligned glass fibre composite materials, *J. Mater. Sci.* **18**, 2798–2810 (1983).
2. P. J. Hogg, A model for stress corrosion crack growth in glass reinforced plastics, *Compos. Sci. Technol.* **38**, 23–42 (1990).
3. H. Kawada and A. Kobiki, A study on stress corrosion cracking using single fiber model specimen (degradation properties of GFRP caused by water absorption), *JSME Int. J. Ser. A* **46**, 303–307 (2003).
4. K. Liao, C. R. Schultheisz and D. L. Hunston, Effects of environmental aging on the properties of pultruded GFRP, *Compos. B* **30**, 485–493 (1999).
5. C. S. Helbling and V. M. Karbhari, Investigation of the sorption and tensile response of pultruded E-glass/vinylester composites subjected to hygrothermal exposure and sustained strain, *J. Reinf. Plast. Compos.* **27**, 613–638 (2008).
6. A. Turon, J. Costa, P. Maimı, D. Trias and J. A. Mayugo, A progressive damage model for unidirectional fibre-reinforced composites based on fibre fragmentation. Part I: formulation, *Compos. Sci. Technol.* **65**, 2039–2048 (2005).
7. M. Kotani, A. Kobiki, Y. Yasufuku and H. Kawada, Strength degradation behavior of glass fiber embedded in single fiber composite under hot water environment, *Trans. Japan Soc. Mech. Eng. Ser. A* **76**, 982–987 (2010) (in Japanese).
8. M. Kotani, Y. Yasufuku, Y. Tamaishi and H. Kawada, Study of strength degradation mechanism of woven GFRP in water environment, *JSME Int. J. Ser. A* (accepted).
9. S. Kimura, J. Koyanagi, D. Yamamoto and H. Kawada, A novel method for evaluation of fiber strength using fragmentation test, *J. Japan. Soc. Exper. Mech.* **6**, 122–127 (2006) (in Japanese).

10. A. B. Morais, Stress distribution along broken fibres in polymer–matrix composites, *Compos. Sci. Technol.* **61**, 1571–1580 (2001).
11. A. B. Morais, Prediction of the longitudinal tensile strength of polymer matrix composites, *Compos. Sci. Technol.* **66**, 2990–2996 (2006).
12. K. Liao and Y. M. Tan, Influence of moisture-induced stress on *in situ* fiber strength degradation of unidirectional polymer composite, *Compos. B* **32**, 365–370 (2001).
13. S. Kimura, Evaluation of mechanical property of fiber–matrix interface in PMC, *PhD Thesis*. Waseda University, Japan (2009).
14. J. Koyanagi, H. Hatta, M. Kotani and H. Kawada, A comprehensive model for determining tensile strengths of various unidirectional composites, *J. Compos. Mater.* **43**, 1901–1914 (2009).